

Supporting Information

Nanoconfinement Controls Mechanical Properties of Elastomeric Thin Films

Pei Bai¹, Mingchao Ma¹, Li Sui², and Yunlong Guo^{1*}

¹University of Michigan – Shanghai Jiao Tong University Joint Institute, Shanghai Jiao Tong University, Shanghai 200240, China

²School of Mechanical Engineering, Beijing Institute of Technology, Beijing 100081, China

*To whom correspondence may be addressed.

Email: yunlong.guo@sjtu.edu.cn.

Supplementary Text

Thickness Determination

The film thickness is measured by AFM. Part of the film was scraped off from the substrate with a sharp blade. The height difference from the substrate without film to the top of the flat film represents the thickness of the film. An example is shown in Fig. S3.

Strain Determination

The film expands or contracts following a periodic manner under the alteration of air pressure, and the real-time topography changes were recorded by the high-speed camera. By the MATLAB coding tool, projection of the centerline of the film, i.e., the side profile of the sample, is successfully extracted from the image, as illustrated by Fig. S4. A microscope calibration glass is used to establish the relationship between pixels of the pictures captured by the high-speed camera and actual sizes, so actual side-view profile of the polymer film could be determined. After that, we perform circular curve fitting on the side profile of the film to get the radius R of curvature. According to the Eq. 2, the strain-time curve is obtained (Fig. S5). In some cases, due to the influence of gravity or the pre-loaded stress, the central position of the membrane in vibration is below the viewing plane (also seen from Movie S2). Therefore, the max strain mentioned in Fig. 3D should be defined as the sum of the pre-strain and strain amplitude in the same direction, as indicated in Fig. S6.

Stress Determination

According to Eq. 1, the stress on the film can be directly derived from the pressure data, with the input of R . For examples, a sine waveform of the stress can be obtained from a sine waveform of the gas pressure in the chamber (Fig. S7A), which represents the dynamic mechanical testing; a triangle waveform of the stress can be obtained from a triangle waveform of the gas pressure in the chamber (Fig. S7B), which represents the biaxial stretching-contraction testing. In the sine-wave case, a sine curve fitting was conducted on the stress-time curve to get the exact stress-time equation (Fig. S7A). In the triangle-wave case, the stress-time curve remains unfitted and combines with the strain-time curve to directly depict the stress-strain curve.

The Sine-waveform Test Mode (Dynamic Mechanical Analysis)

Here we show some representative results to illustrate how does the sine-wave test mode work. The stress-time curve and strain-time curve are obtained just to follow the procedures described above and they are all sinusoidal in this work. Integrating them into single picture require the clock synchronization: the myRIO-1900 device activates the data recording of pressure sensor and high-speed camera at the same time. Sharing the same starting point triggered by the myRIO-1900, the pressure sensor and the high-speed camera follow their sampling pace, both controlled by crystal oscillators, to record the data respectively. An example of resultant stress-time curves and strain-time curves is represented in Fig. S8. By directly comparing the two fitted curves in this figure, the phase difference of the two sine curves can be determined (Fig. S8). According to Eq. 5 - 8, σ_0 and ε_0 can be determined by the amplitudes of the stress-time and strain-time curves, respectively. Finally, the biaxial storage modulus E'_{bi} , the biaxial loss modulus E''_{bi} , and the loss factor $\tan \delta$ all can be obtained.

The Master Stress-strain Curve from Triangle-waveform Mode

Here we show some representative results to illustrate how does the biaxial stretching and contraction data analysis work. Followed similar procedure as the sine-wave test mode, the stress-time curve and the strain-time curve share the same timeline with each other. Therefore, we can integrate two curves into a stress-strain curve. However, due to the travel limitation of the voice coil motor, the air pressure range in each experiment and the resulting stress and strain range are also limited, which means we cannot attain a stress-strain curve in a large range from a single experiment. As a result, multiple sets of experimental results, with different initial air pressures with almost the same amplitude, are combined to form a master curve of the stress-strain response. An example is shown in the Fig. S9.

Additional Mechanical Testing Results

Here we will give some representative results in the Fig. S10 - S15. As mentioned in the report, the sine curve fit results of the Fig. 1E were given here: the stress-time fitted curve has an adjusted R-Square of 0.996 at the 95% confidence level; the strain-time fitted curve has an adjusted R-Square of 0.999 at the 95% confidence level.

Simulations of Pressure Distribution

In the micro-vibration testing, we assume that the instant pressure measured by the sensor is equal to the pressure exerting on the film. To confirm this assumption, and to guide experimental on the upper bound of the applicable frequency, and to determine the possible phase delay between the pressure sensor and the thin film, we calculated the pressure distribution inside the chamber by using ANSYS CFX Student Version.

The 3D model was constructed in SolidWorks as shown in Fig. S16. The dimensions of the model are the same to that introduced in the apparatus section. The sizes of chamber are 12 mm in length, 12 mm in width, and 6 mm in height. Thin film locates at the center of the top surface. The length and diameter of the channel between chamber and pressure sensor are 3 mm and 2 mm, respectively. Pressure sensor locates at the center of the end of this channel. The channel (2 mm in diameter) on the bottom of chamber is connected with a piston. The length of the bottom channel is 5 mm, which is long enough to control the pressure in chamber by the motion of piston.

The 3D model was then imported to CFX after meshing. Blanco and coworkers demonstrated that air can be considered as ideal gas when pressure deviate from atmospheric pressure within 10 kPa with temperature changing from 22 °C to 49 °C.^{S1} In our experiments, pressure is lower than 600 Pa and temperature is around 25 °C. As such, the gas in our chamber can be regarded as ideal gas. The experiments can be regarded as under isothermal conditions, as the temperature deviation in the chamber is negligible. The mesh motion of piston is controlled by specified displacement according to the following equation:

$$d = d_0 \sin(2\pi ft) \quad (S1)$$

where d_0 , which is 1.654 mm, determined by the maximum pressure in the chamber. f is the frequency of input pressure. Transient results were simulated under specific timesteps.

When the input pressure is 1-Hz (the real frequency in our experiments) sine-wave driven by syringe, the Reynolds number is lower than 2 according to the dimensions (much lower than the laminar flow upper bound 2300). Consequently, turbulence is not involved in the simulation. The timesteps of transient simulation are set to be 0.01 s. Then, the pressure distribution in the chamber is simulated by CFX-Solver Manager and a representative pressure distribution is presented in Fig. S17. We monitored the predicted pressures at the center of thin film and pressure sensor, and the results are shown in Fig. S18. The predicted pressure is fitted by sinusoidal function, as expressed by Eq. S2:

$$P(t) = P_0 \sin(\omega t + \delta) + b \quad (\text{S2})$$

The parameters of two curves are summarized in Table S1. Two fitted curves are overlapped. The maximum pressure deviation between the thin film and the pressure sensor ($\text{Max } |P_{\text{thin film}} - P_{\text{sensor}}|$) is only 2.45×10^{-4} Pa. According to the fitted parameters, phase delay does not exist. As such, we conclude that our experimental system is reliable and the pressure detected by the sensor can represent the pressure at the film (i.e., the air under our experimental conditions behaves incompressible).

To check the robustness of our experiments, we simulate the pressure distribution at various high frequencies. When input pressure is 500 Hz sine-wave, the Reynolds number is approximate to be 5.2. The fluid is still a laminar flow. The timesteps are set to be 2×10^{-5} s. The pressure distributions at the beginning of the first and second period are illustrated in Fig. S19. At the beginning of the first period, apparent pressure gradient exists in the chamber. However, the system becomes stable from the second period. Pressure gradient is very small. The corresponding simulation results at the film and the sensor are illustrated in Fig. S20. The pressure is fitted from the second period, and the fitted parameters are listed in Table S2. Two fitted curves are apparently overlapped. The maximum pressure deviation between the thin film and the pressure sensor in the second period is 0.604 Pa. From the fitted parameters, the phase delay is 0.2 ms, which is much less than the sampling rate of our experiments. Therefore, we believe that our system is still reliable on high frequencies, at least for 500 Hz.

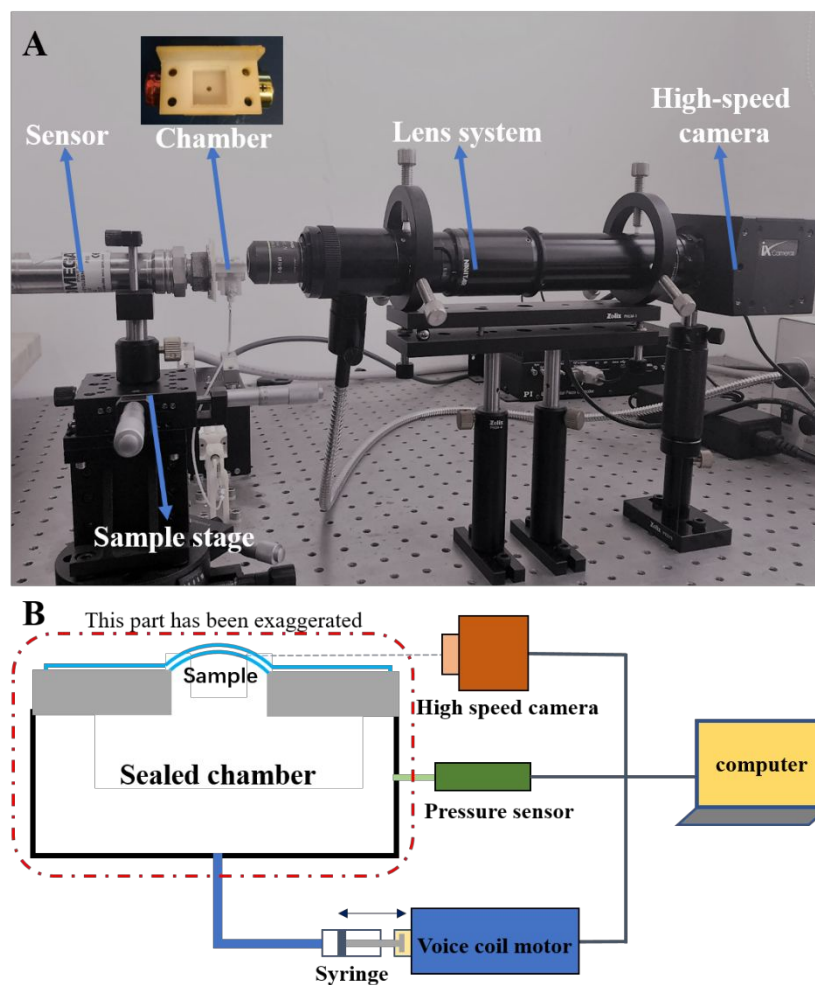


Fig. S1. (A) Image and (B) schematic of the experimental setup showing the high-speed camera, sealed chamber, pump system, and sample stage. The inset in the upper left in panel (A) shows the chamber (in white). The dimensions of the internal space of the cuboid chamber are 12 mm in length, 12 mm in width, and 6 mm in height.

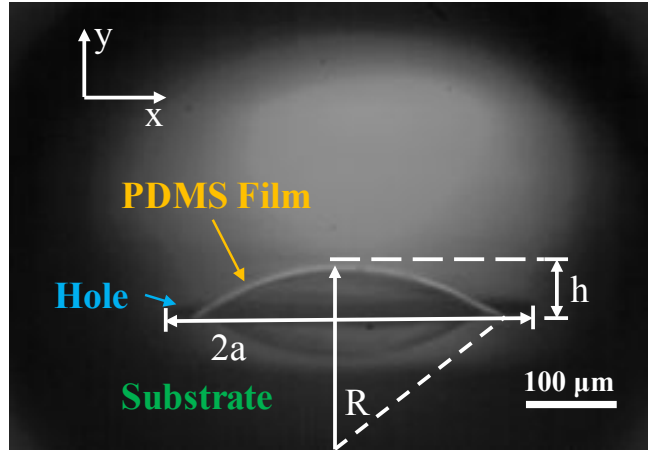


Fig. S2. Bulging profile of a PDMS film with thickness of 125 nm, under a pressure of 645 Pa. The contour line of the PDMS bubble is a part of a circle with radius R . The radius of the hole represented by a is 200 μm (fixed hole on the top wall of the chamber). For the profile shown in this image, h is about 64 μm , and R is 345 μm .

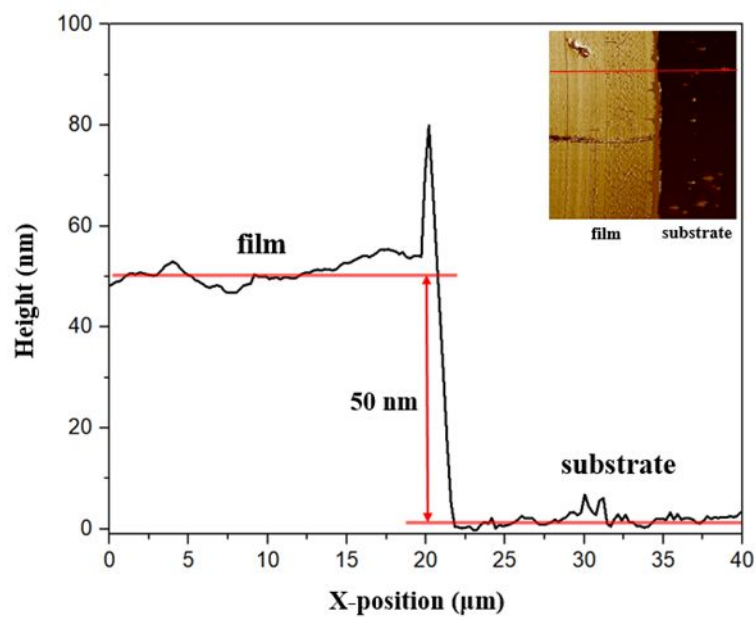


Fig. S3. An AFM scan over the stage between the PDMS film and glass substrate.

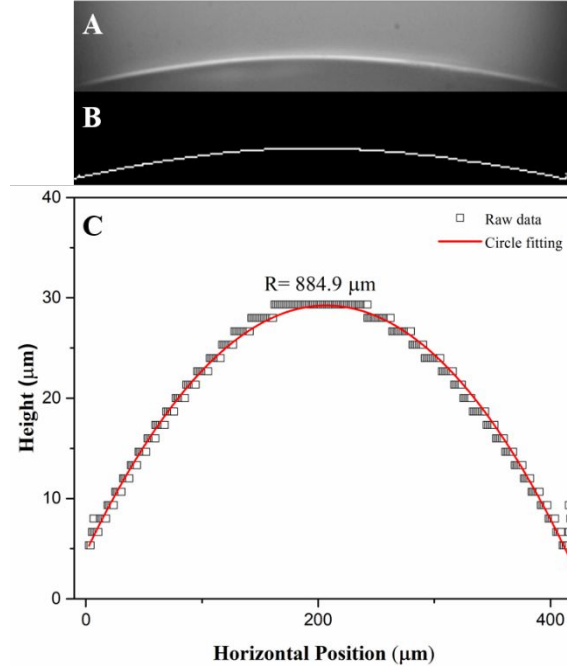


Fig. S4. Image processing and strain determination

(A) A cropped image of a PDMS thin film with the thickness of 50 nm. (B) The contour line was extracted from (A) by the MATLAB coding. (C) The contour line was digitalized (open squares) and the radius of the curvature was obtained after curve fitting ($R = 884.9 \mu\text{m}$). The red line was a circle fitting of the contour line ($R^2 = 0.992$, with 95% confidence level).

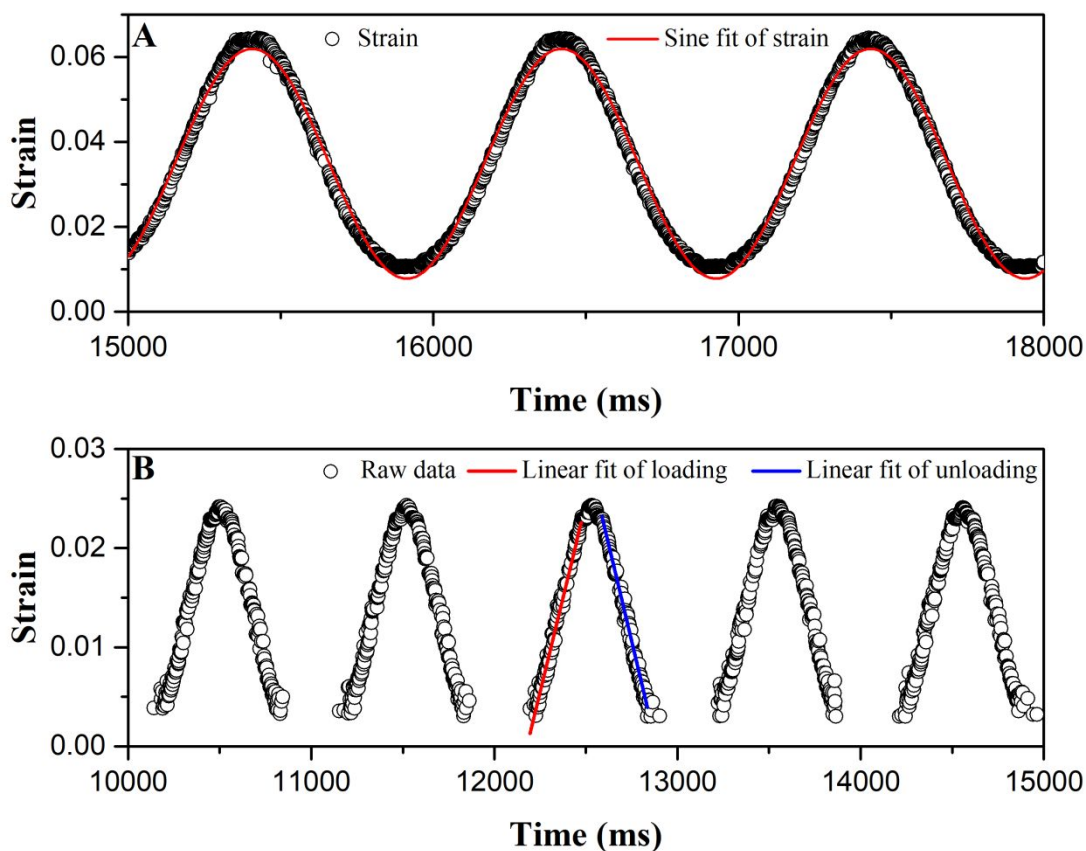


Fig. S5. Strain determinations for the sine-wave test mode and the biaxial stretching test mode.

(A) The strain-time curve (open circles) and the sine curve fitting (red line, $R^2 = 0.990$ with 95% confidence level) for a PDMS thin film with thickness of 125 nm. (B) The corresponding figure for the biaxial stretching-contraction test mode. The linearity was examined respectively for the loading and unloading processes ($R^2 = 0.987$ for the red line and $R^2 = 0.993$ for the blue one, both with 95% confidence levels).

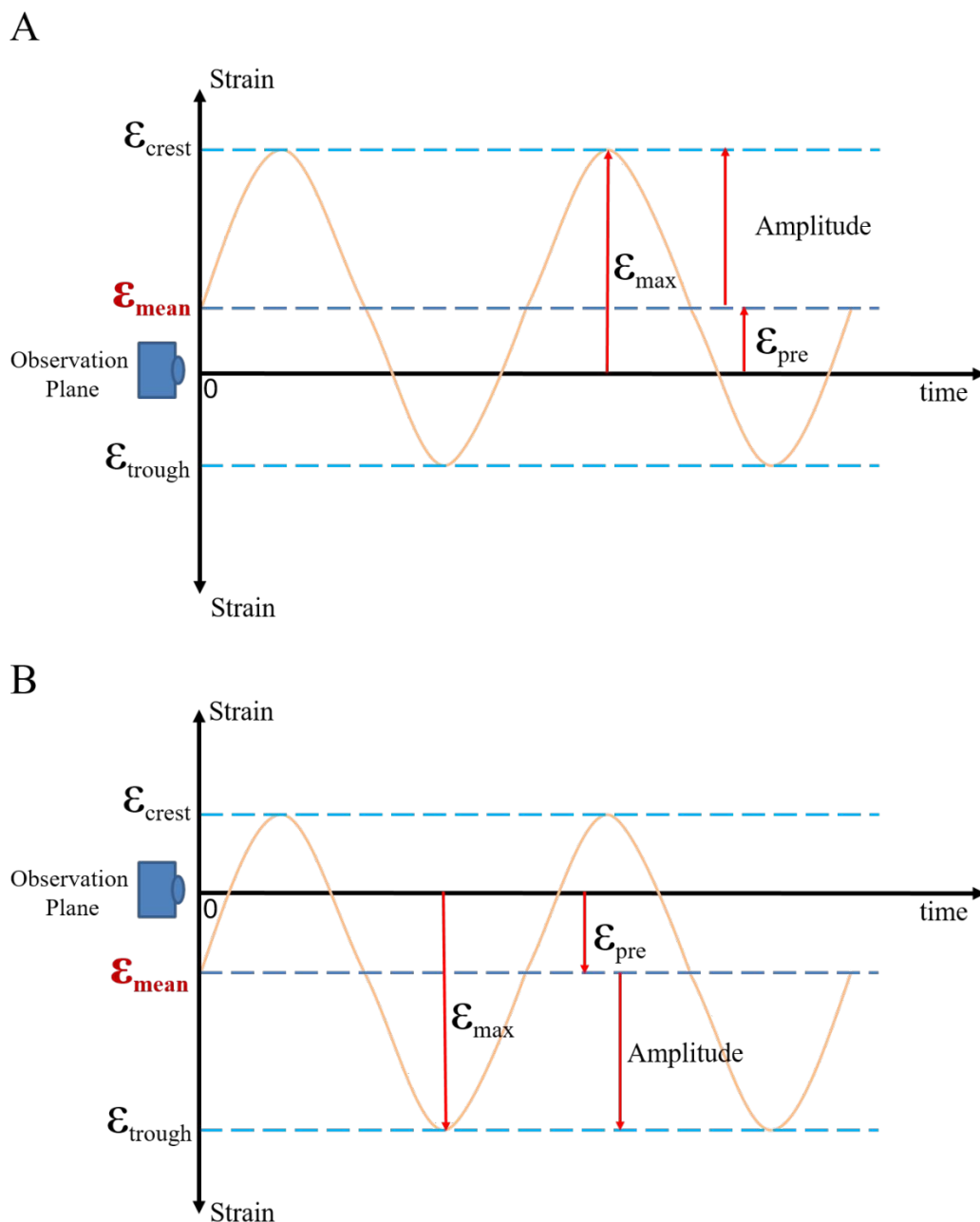


Fig. S6. Schematic of the max strain calculation.

(A) The central position (ϵ_{mean}) of the film is higher than the observation plane. In this case, the max strain just equals to the strain value of the wave crest. (B) The central position (ϵ_{mean}) of the film is lower than the observation plane. In this case, the max strain just equals to the strain value of the wave trough.

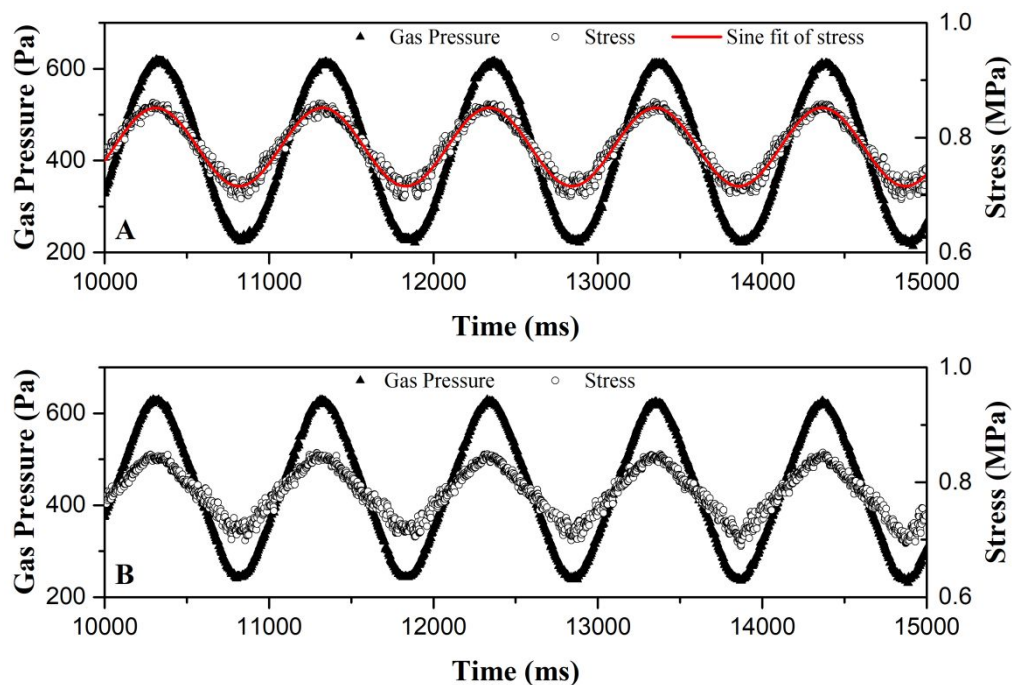


Fig. S7. Stress determinations for the sine-wave test mode and the biaxial stretching mode.

(A) The pressure-time curves (black triangles) and corresponding stress-time curves (open circles) for the sine wave test mode (a PDMS thin film with 125 nm). The red line is the sine curve fit for the stress-time curve ($R^2 = 0.976$, with 95% confidence level). (B) The gas pressure and stress data of the biaxial stretching-contraction mode (a PDMS thin film with 125 nm thickness). The stress-time curve remains unfitted.

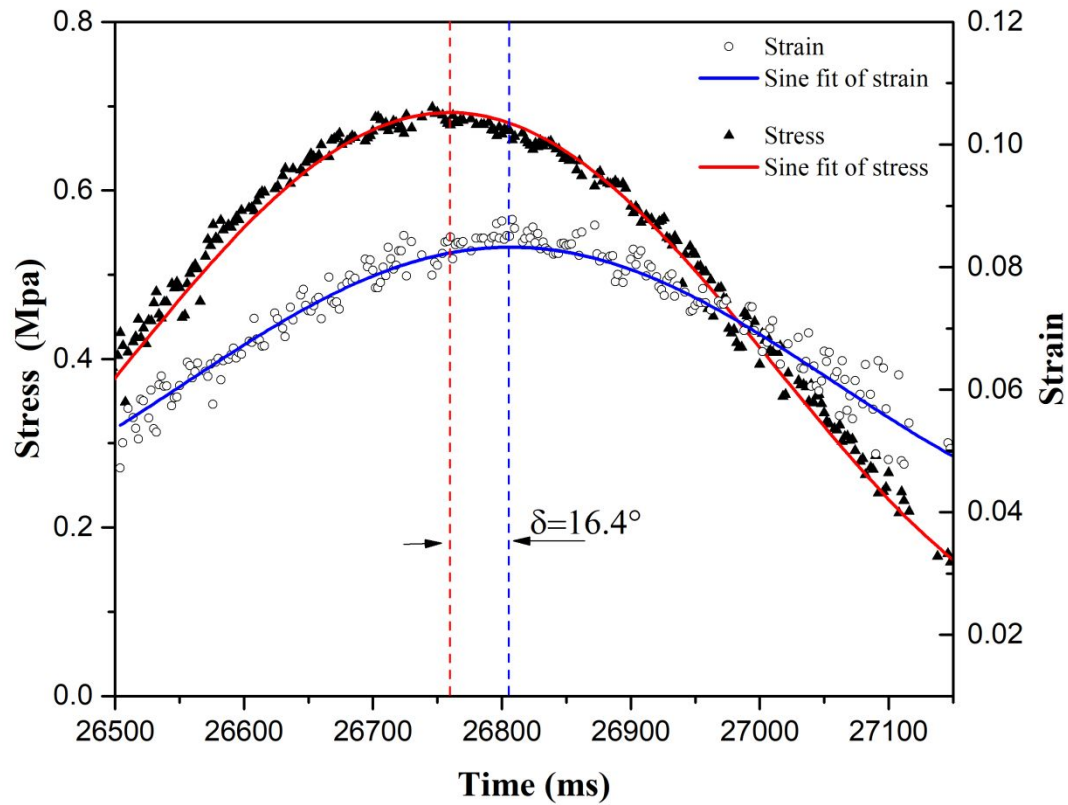


Fig. S8. Details of stress and strain in dynamic mechanical testing of a 125-nm PDMS thin film.

The Stress-time (black triangles) and the strain-time curve (open circles) are plotted in this figure. After being sine fitted respectively (the red line for the stress and the blue line for the strain), two symmetry axes are drawn (the red dash line for the stress and the blue one for the strain) and the phase shift information ($\delta = 16.4^\circ$) can be directly determined ($R^2 = 0.987$ for the stress and $R^2 = 0.938$ for the strain respectively, both with 95% confidence levels).

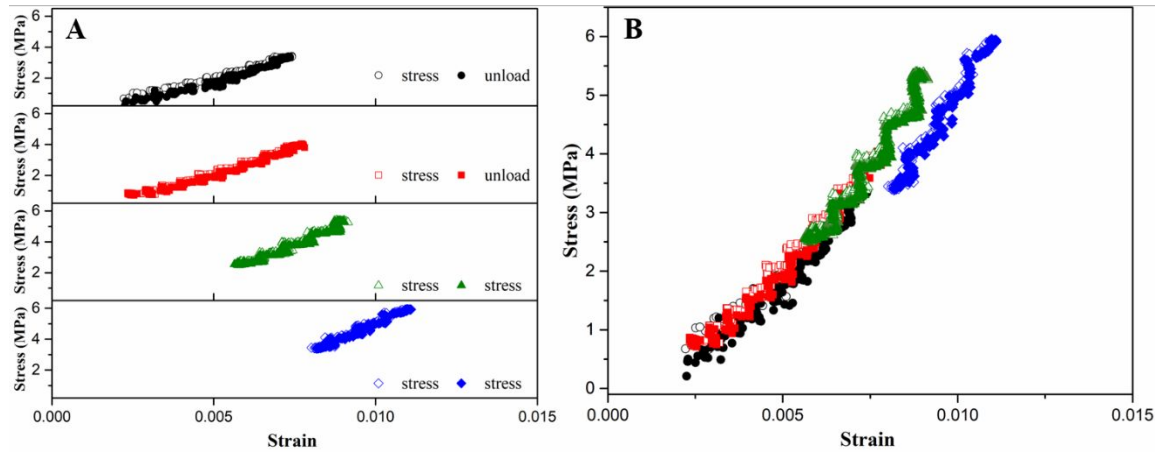


Fig. S9. The master stress-strain curve is determined from four individual stress-strain curves. No horizontal or vertical shift applied.

(A) Stress-strain curves of a PDMS film with 50 nm thickness at different strain ranges. (B) The master stress-strain curve.

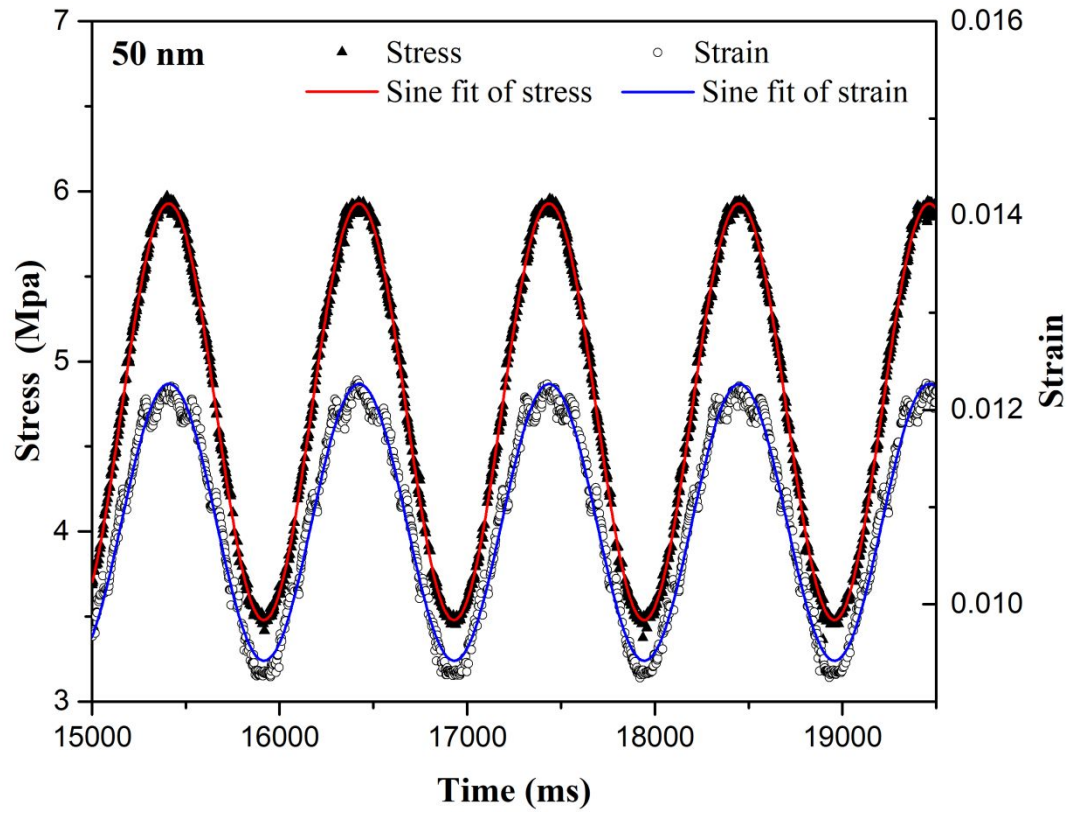


Fig. S10. A sine wave test of a PDMS thin film with the thickness of 50 nm.

There is no significant phase difference ($\sim 0^\circ$) between the stress and strain curves. ($R^2 = 0.999$ for the stress sine fit and $R^2 = 0.979$ for the strain sine fit, respectively, with 95% confidence levels).

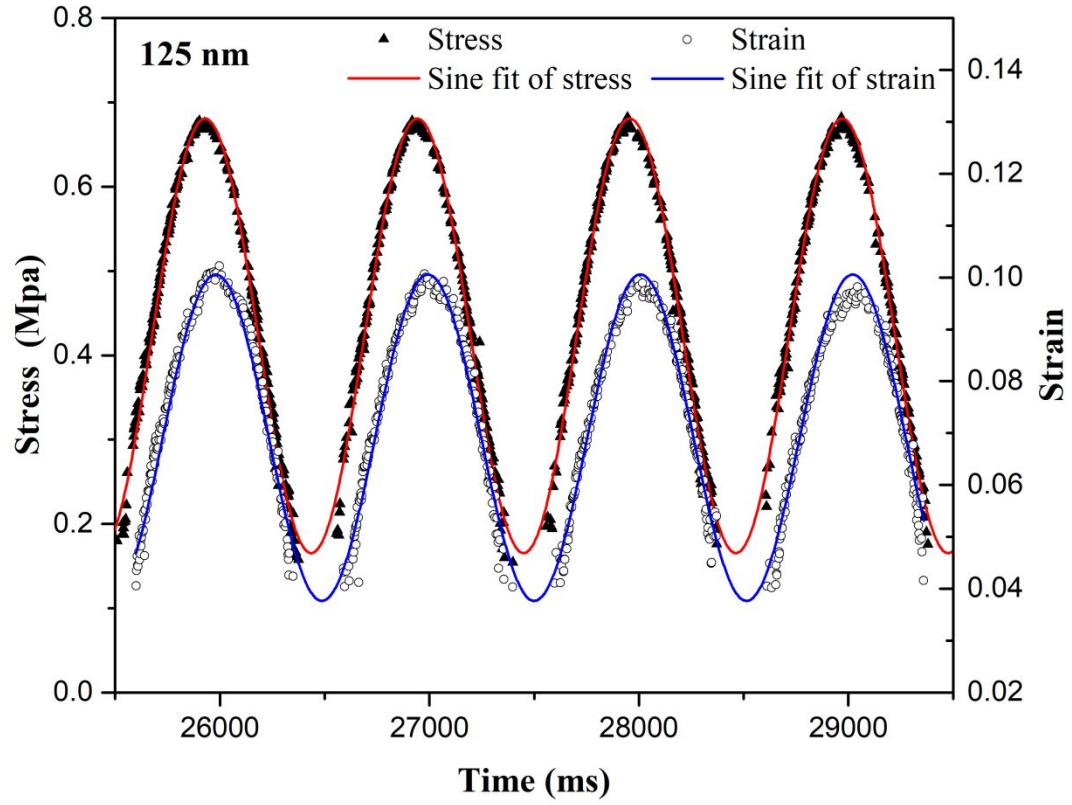


Fig. S11. A sine wave test of a PDMS thin film with the thickness of 125 nm.

The phase difference between the stress and strain curves is 17.9° . ($R^2 = 0.981$ for the stress sine fit and $R^2 = 0.975$ for the strain sine fit, respectively, with 95% confidence levels).

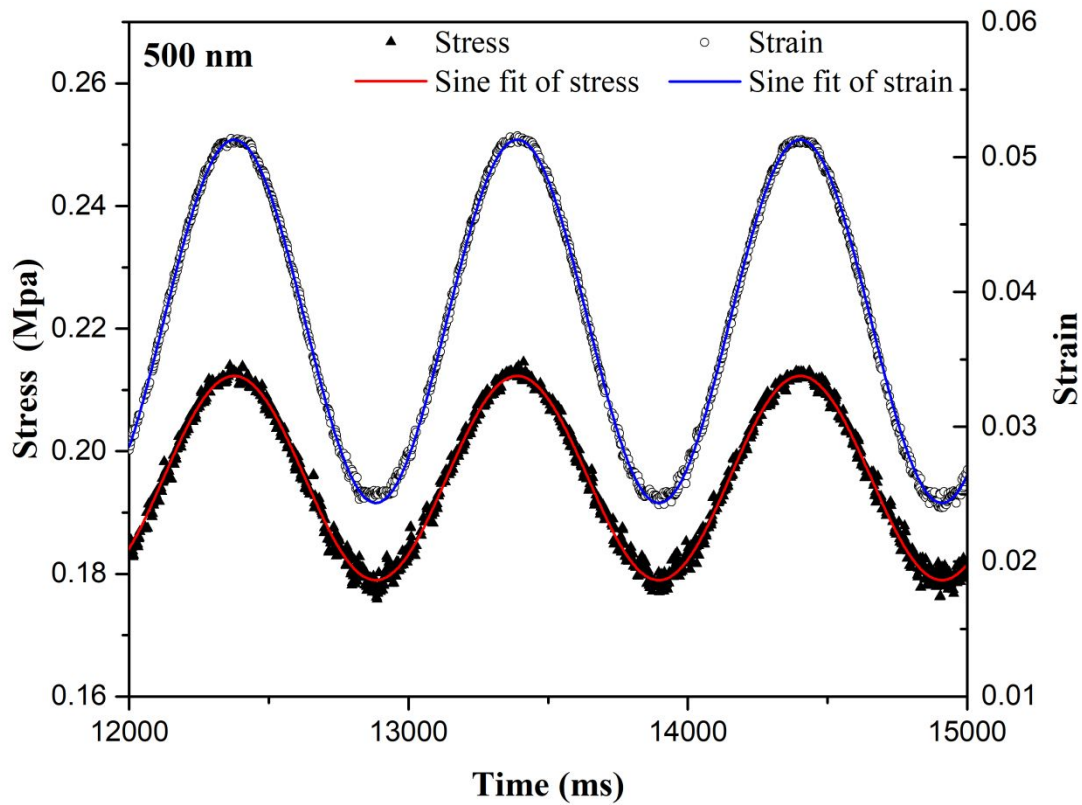


Fig. S12. A sine wave test of a PDMS thin film with the thickness of 500 nm.

The phase difference between the stress and strain curves is negligible. ($R^2 = 0.992$ for the stress sine fit and $R^2 = 0.999$ for the strain sine fit respectively, with 95% confidence levels).

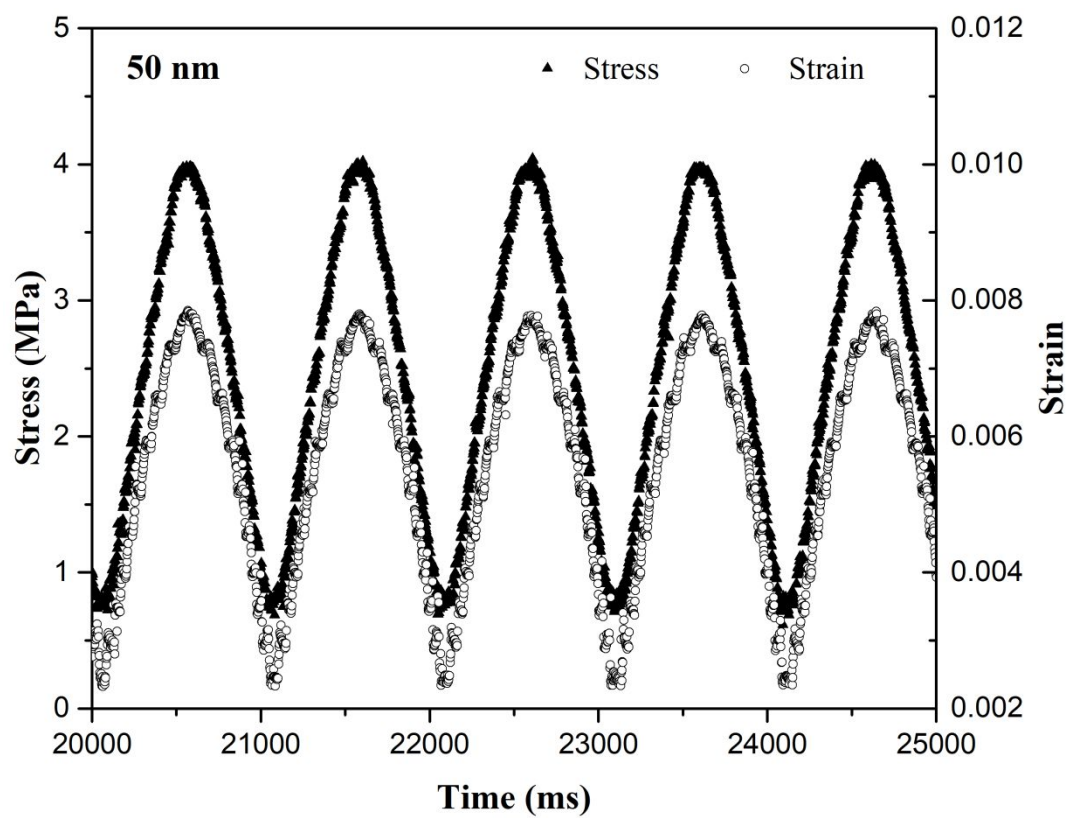


Fig. S13. A triangle wave test of a PDMS thin film with the thickness of 50 nm.

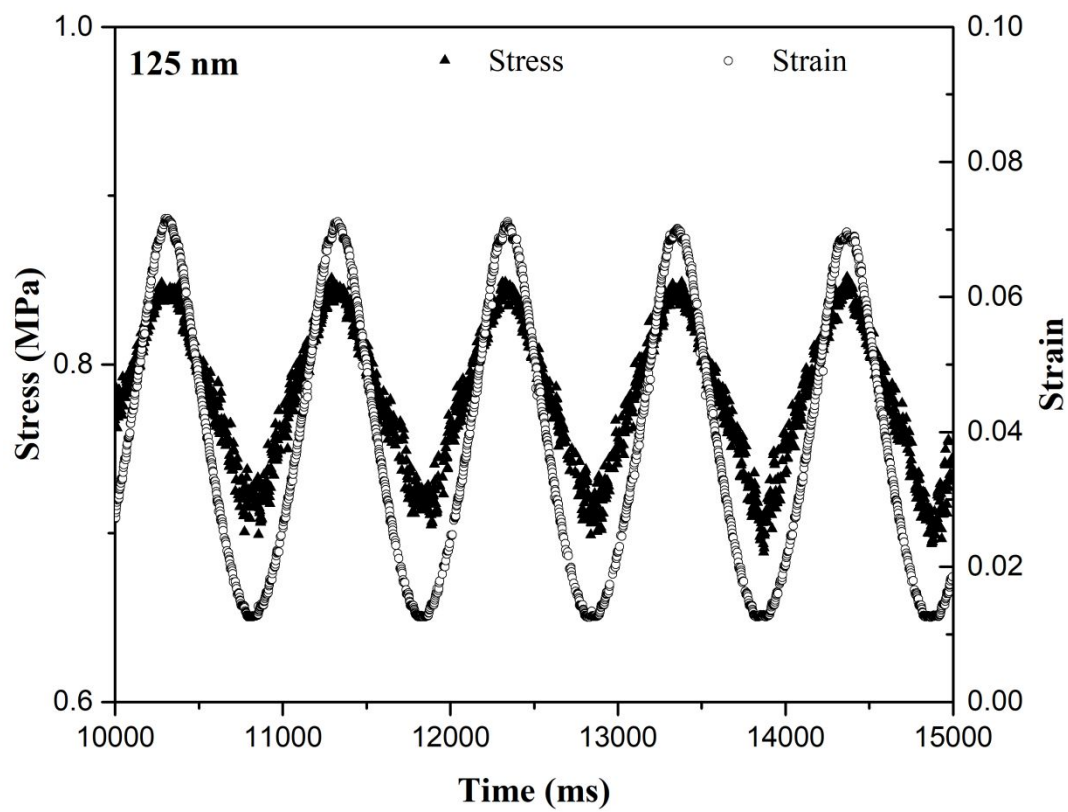


Fig. S14. A triangle wave test of a PDMS thin film with the thickness of 125 nm.

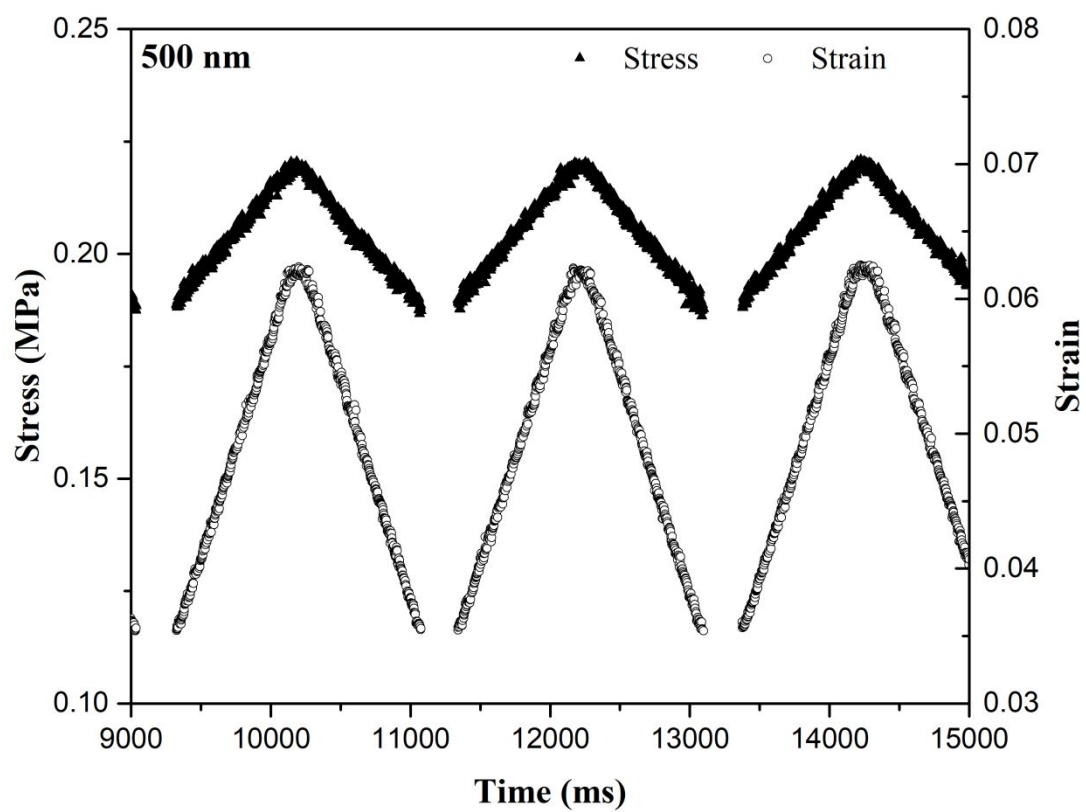


Fig. S15. A triangle wave test of a PDMS thin film with the thickness of 500 nm.

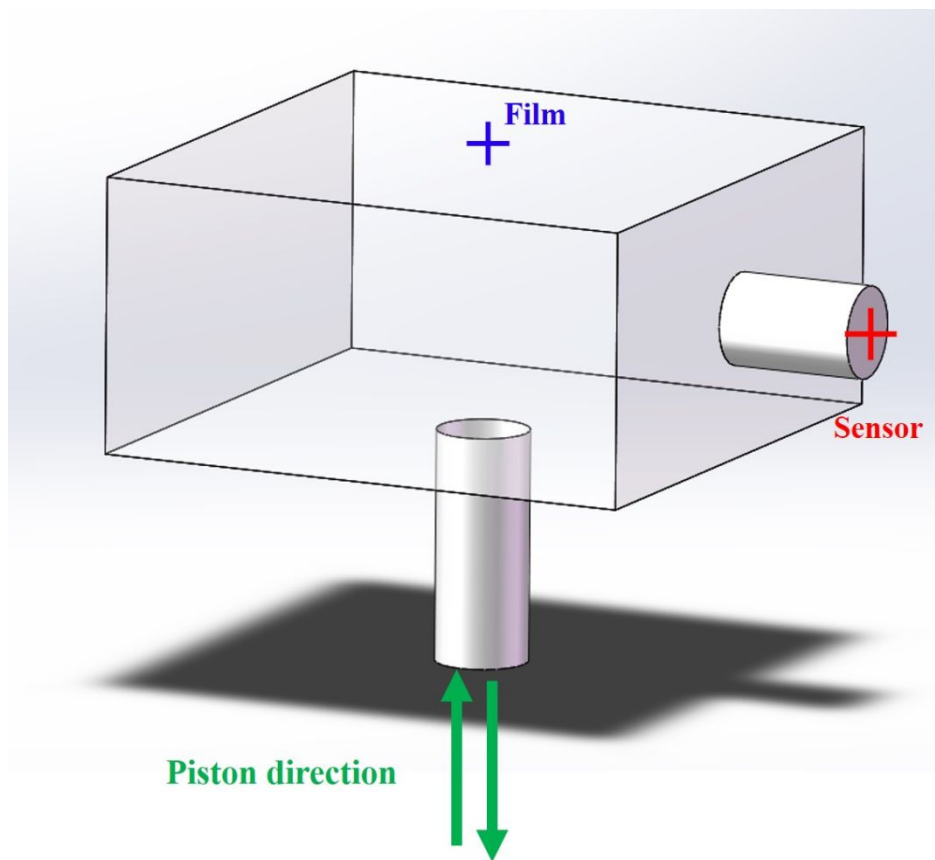


Fig. S16. The 3D model for ANSYS simulation.

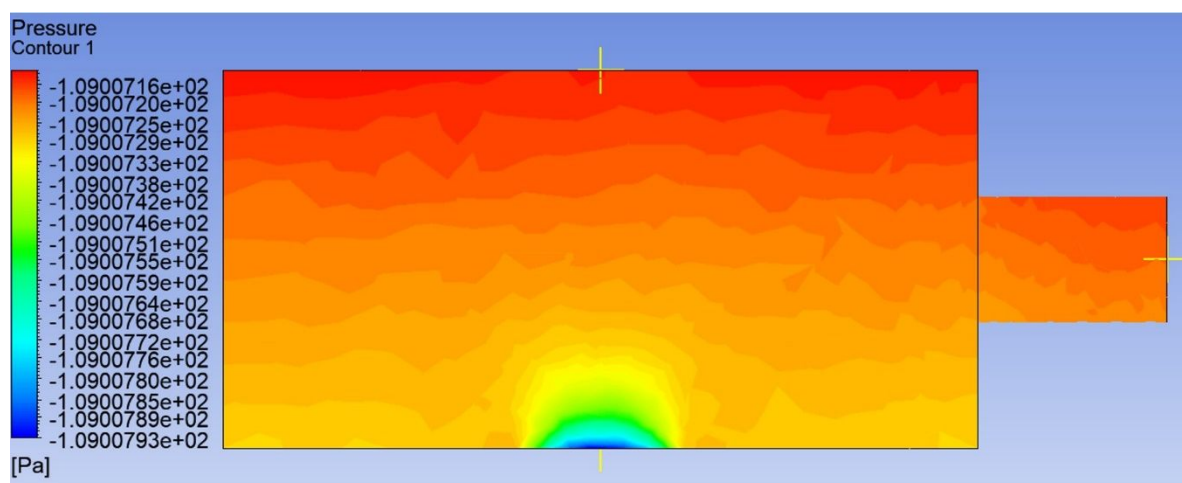


Fig. S17. A representative pressure distribution in the chamber at 1 Hz.

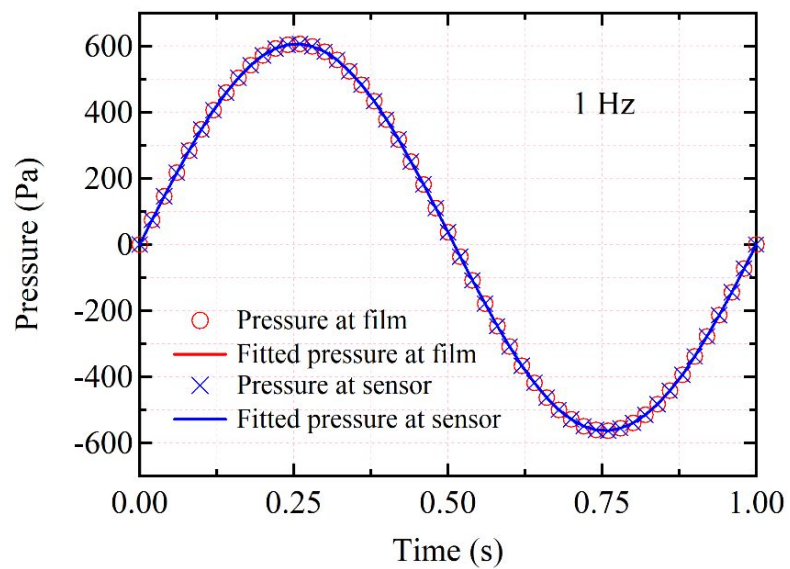


Fig. S18. The simulated pressures at the center of thin film and at the location of the pressure sensor at 1 Hz. Two fitted curves are overlapped.

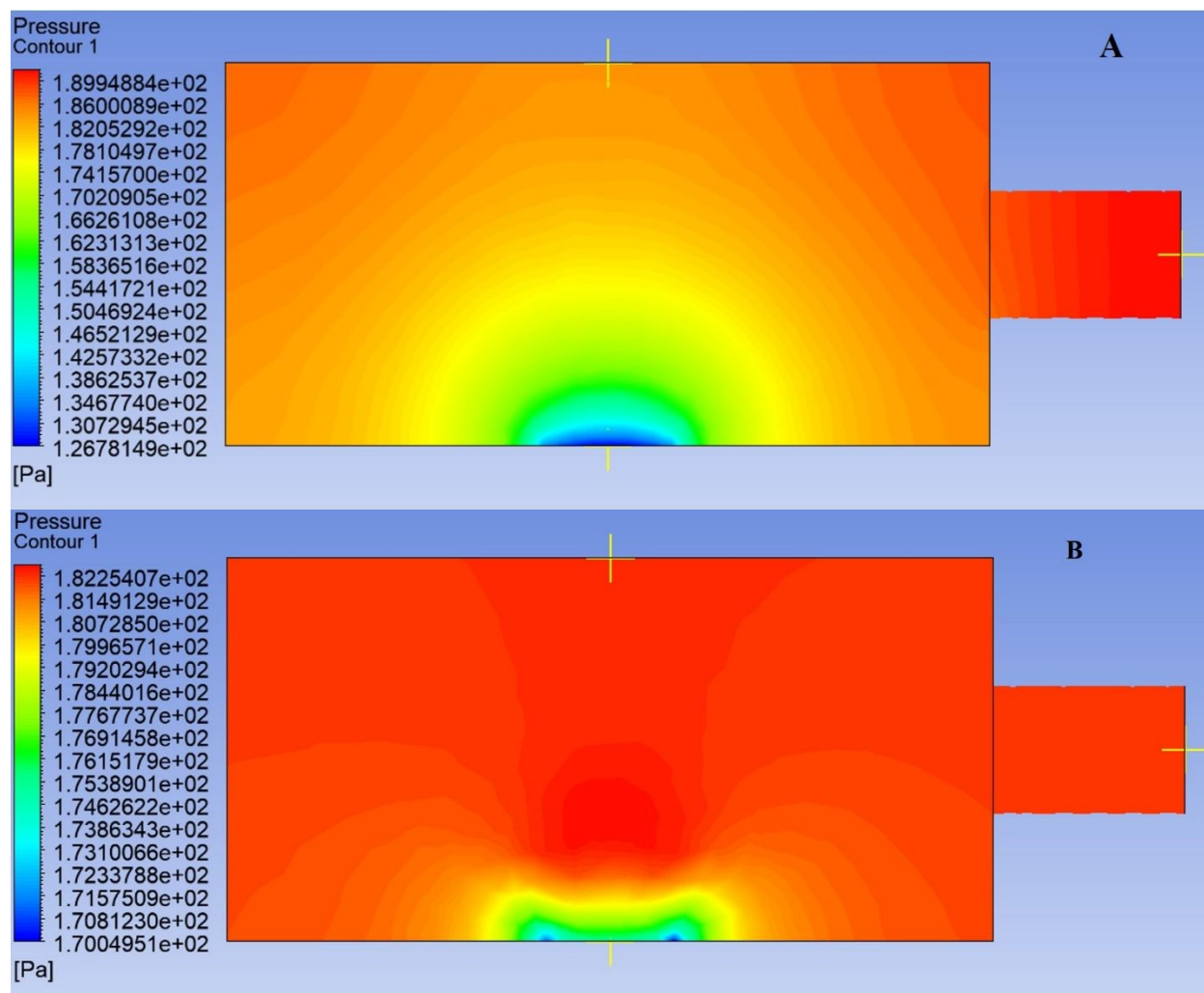


Fig. S19. A representative pressure distribution in the chamber at 500 Hz.

(A) 0.0001 s after the beginning of the first period. (B) 0.0001 s after the beginning of the second period.

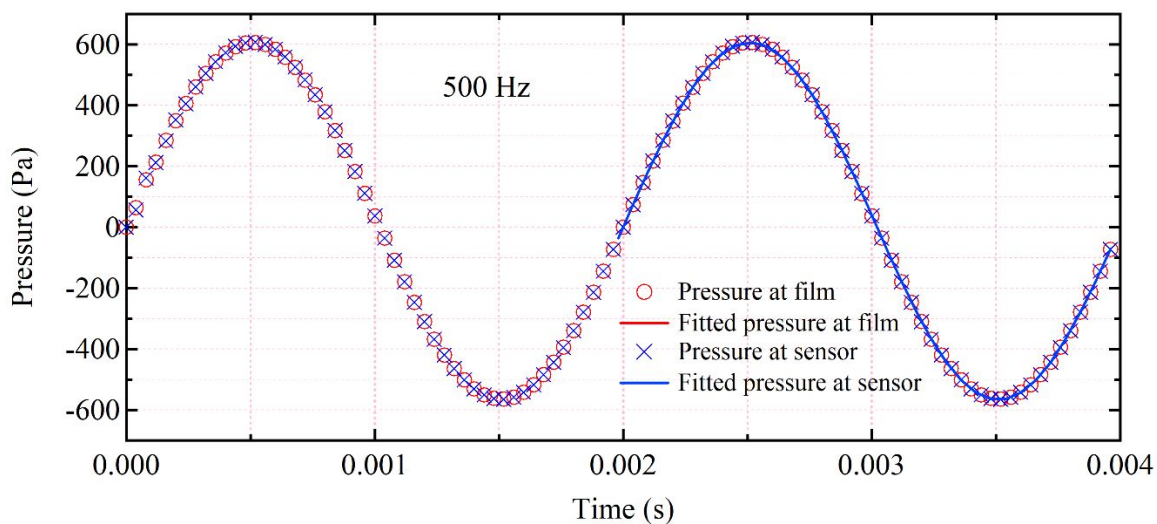


Fig. S20. The simulated pressures at the center of thin film and at the location of the pressure sensor at 500 Hz. Two fitted curves are overlapped from the second period.

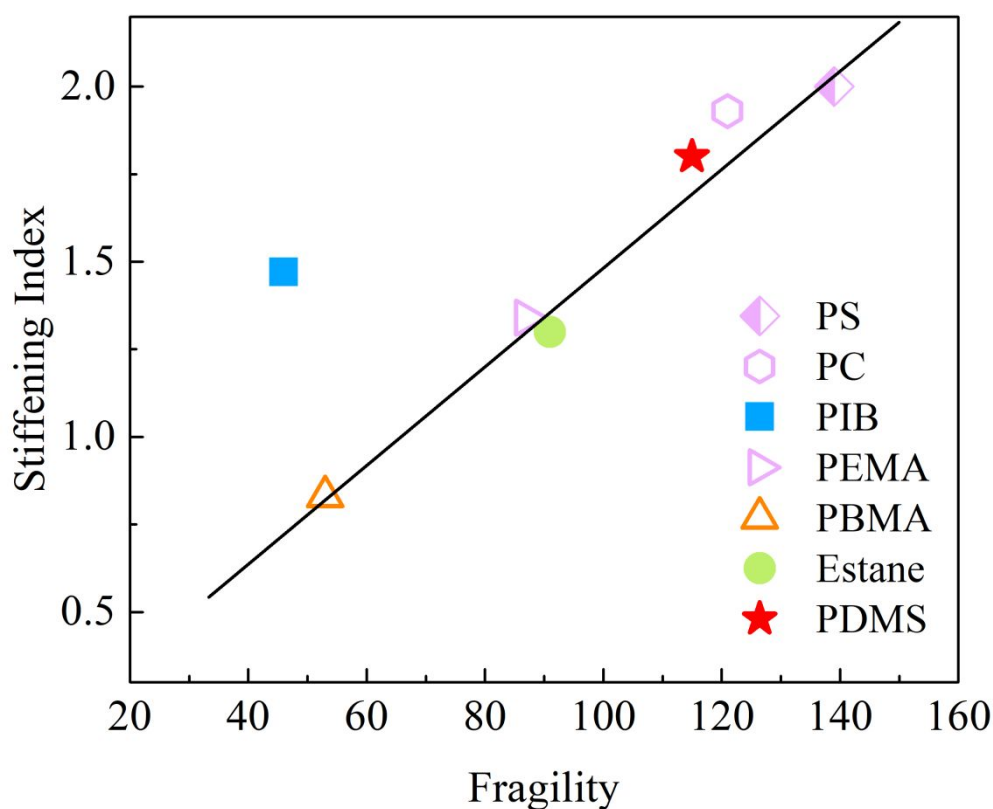


Fig. S21. Rubbery stiffening index versus dynamic fragility index for several materials. The black line is reproduced from the linear fitting curve in the McKenna Group's work.^{S2} The red

star is the data point of PDMS in this work. Fragility index of PDMS of 115 is taken from literature. ^{S3}















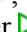
Table S1. Fitting parameters for the simulated pressures at the center of thin film and at the location of the pressure sensor at 1 Hz.

Position	P_0	ω	δ	b
Thin film	584.5919	6.2835	-0.0316	20.0363
Sensor	584.5921	6.2835	-0.0316	20.0363

Table S2. Fitting parameters for the simulated pressures at the center of thin film and at the location of the pressure sensor at 500 Hz.

Position	P_0	ω	δ	b
Thin film	585.8342	3141.7795	-0.0322	19.9537
Sensor	586.3918	3141.7751	-0.0324	19.9050

Table S3. Correspondence between data points and literature in Fig. 4C and 4D.

Data Set	Citation Source	Reference No.
PS 	P. A. O'Connell et al., Journal of Polymer Science Part B: Polymer Physics 46, 1952 (2008)	20
PC 	P. A. O'Connell et al., Macromolecules 45, 2453 (2012)	11
PEMA 	X. Li et al., Macromolecules 48, 6329 (2015)	19
PBMA 	S. Xu et al., The Journal of Chemical Physics 132, 184902 (2010)	21
PIB 	H. Yoon et al., Macromolecules 50, 9821 (2017)	12
Ethane 	M. Zhai et al., Polymer 55, 2725 (2014)	18
PS 	J. Chang et al., Macromolecules 51, 6764 (2018)	15
PS _{114K}  , PS _{1800K}  , PMMA 	C. M. Stafford et al., Macromolecules 39, 5095 (2006)	14
PS 	Y. Liu et al., Macromolecules 48, 6534 (2015)	7
P3HT 	R. Song et al., Macromolecules 53, 1988 (2020)	16
PS _{151K}  , PS _{1049K} bilayer  , PS _{1049K} single layer 	P. M. Yiu et al., ACS Macro Letters 9, 1521 (2020)	22

Movie S1.

This movie shows the triangle wave test process of 50 nm thick PDMS film. The test strain varies from 0.8% to 1.2%, and the test frequency is 1 Hz.

Movie S2.

This movie shows the sinusoidal wave test process of 125 nm thick PDMS film. The strain varies from 0 to 3%, and the test frequency is 1 Hz.

Movie S3.

This movie shows the triangle wave test process of 500 nm thick PDMS film. The strain varies from 2.4% to 5.2%, and the test frequency is 0.5 Hz.

SI References

- S1. Blanco, L. H.; Romero, C. M., A systematic experimental test of the ideal gas equation for the general chemistry laboratory. *Journal of Chemical Education* **1995**, 72, 933-936.
- S2. Yoon, H.; McKenna, G. B., “Rubbery stiffening” and rupture behavior of freely standing nanometric thin PIB films. *Macromolecules* **2017**, 50, 9821-9830.
- S3. Hintermeyer, J.; Herrmann, A.; Kahlau, R.; Goiceanu, C.; Rössler, E.A., Molecular weight dependence of glassy dynamics in linear polymers revisited. *Macromolecules* **2008**, 41, 9335-9344.